 FDMP, vol.13, no.1, pp.1-17, 2017

Control of the Convective Flow Instabilities in a Simulated Czochralski Growth System

N. Soltani[1] and S. Rahal[1]

Abstract: A three-dimensional time-dependent numerical study of the flow instabilities in a simulated Czochralski system is conducted. The comparison with previously published experimental results is reported. The simulations were performed using a refined grid in order to investigate flow instabilities in the crucible. Simulations have been carried out for various crystal rotational speeds, by taking into account the effects of Rayleigh and Marangoni numbers. The temperature fluctuations near the crystal/liquid interface are analyzed. The method used for that purpose is the Fast Fourier Transform with the corresponding spectra. From numerical simulations, it has been observed that for rotational speeds of the crystal less than 10 rpm, the temperature fluctuations are increased until a magnitude of 1.1 K over a period of 6 min. For crystal speeds larger than 10 rpm the fluctuations are extremely reduced to a magnitude less than 0.02 K.

Keywords: Czochralski method, crystal growth, flow instabilities, convection, numerical simulation.

Nomenclature

g =	*Gravity, m s^{-2}*
H =	*Height, m*
h =	*heat transfer coefficient, W m^{-2}K^{-1}*
Ma =	*Marangoni number*
P =	*Pressure, Pa*
Pr =	*Prandlt number*
r =	*Radial coordinate*
Ra =	*Rayleigh number*
R_{cru} =	*Radius of the crucible, m*
R_{cry} =	*Radius of the crystal, m*
Re =	*Reynolds number*
T =	*Temperature, K*

[1] LESEI Laboratory, Department of Mechanical Engineering, University of Mostefa Ben Boulaid Batna2, 53, Fésdis, Batna 05078, ALGERIA. n.soltani@univ-batna2.dz

t =	*Time, s*
u, v, w =	*Velocity components, m s^{-1}*
z =	*Axial coordinate*

Greek symbols

α =	*Thermal diffusivity, m^2 s^{-1}*
β =	*Volumetric coefficient of thermal expansion, K^{-1}*
μ =	*Dynamic viscosity, kg m^{-1} s^{-1}*
λ =	*Thermal conductivity, W m^{-1} K^{-1}*
ν =	*Kinematic viscosity, m^2 s^{-1}*
θ =	*Azimuthal coordinate*
ρ =	*Density, kg m^3*
σ =	*Surface tension, N m^{-1}*
$\frac{\partial \sigma}{\partial T}$ =	*Surface tension variation as function of the Temperature, N m^{-1} K^{-1}*
ΔT =	*Difference of temperature applied between the crucible and the crystal, K*
Ω_{cry} =	Crystal rotational speed, rpm

Subscript

a =	Ambiant
cru =	Crucible
cry =	Crystal

1 Introduction

The Czochralski (Cz) method is one of the most important methods for producing silicon single crystals from the melt. In this method, heat and mass transfer in the crucible are strongly influenced by the melt convection driven by various forces, such as the buoyancy force, the centrifugal forces due to crystal and crucible rotations, as well as the thermocapillary force induced by the temperature dependence of the surface tension at the melt upper surface see Li, Peng, Shi et al. (2006), for more details. Crystal pulling by the Czochralski method requires strict control of the flow in the melt to obtain crystals with adequate electrical, mechanical and optical properties indeed, velocity and temperature fluctuations encountered in the Czochralski crucible have been identified to be as one of the factors leading to inhomogeneities in the grown crystal. Kanda, Hourai, Miki et al. (1996), studied the effects of melt-temperature fluctuations on growth striations in crystals grown in a commercial-scale growth system by an analysis of the Fast-Fourier-Transform (FFT) method. The period of the growth striations observed in crystals corresponded exactly to that of temperature fluctuations in the melt. Haslavsky, Miroshnichenko, Kit et al. (2011) examined the effect of the slow crystal rotation on three-dimensional oscillatory instability in a Czochralski melt flow. The measurements

confirmed, partially the destabilization of the Czochralski convective flow by a slow rotation. Haslavsky, Miroshnichenko, Kit et al. (2013) developed a new experimental setup that allows measuring oscillatory instability threshold in a Czochralski melt flow model. The critical temperature fluctuation has been significantly reduced under the effect of a weak rotation. Zhong, Jingqiu, Hiroshi (2003) investigated the optimal crystal rotation for LiCAF crystal growth by numerical techniques. The model study (adiabatic bottom) indicates that a relatively but never ideally flat interface is realized by crystal rotation. The critical crystal rotating rate for the convective instability increases with the decrease of the melt height and crystal size. They found an optimal crystal rotation close to 14 rpm for an aspect ratio equal to 1 and $\Delta T = 50$ K.

The effect of Marangoni convection on the flow structure features is investigated, and the results indicated that neglecting Marangoni convection causes a large deviation. Gelfgat (2007) observed the effect of the destabilization of free convective flows by a weak rotation. After studying several models in which flows are driven simultaneously by convection and rotation, it has been concluded that the destabilization is observed in the cases for which centrifugal force acts against the main convective circulation. The effect has been studied by considering a combined convective/rotating flow in a cylinder with a rotating lid and a parabolic temperature profile at the sidewall. Zhang, Zheng, Prasad et al. (1998) have used the RNG k-ε model to simulate the flow in a large crucible (crystals of 300 mm diameters and crucibles of 600 mm or 750 mm diameters). They studied the influence of the rotational speeds. Flow instability of molten Si during Czochralski (CZ) Si crystal growth has been studied by Kakimoto, Watanabe, Eguchi et al. (1994) utilizing a 3D heat and mass-transfer model together with global heat- and mass-transfer calculation. It is found that the phase transition from an axisymmetric to a non-axisymmetric mode of the flow occurs depending critically on the growth parameters, such as temperature distribution, crucible as well as crystal rotation rates.

In this work, we have developed and validated a numerical simulation procedure that allowed studying the convective flow instabilities using the FFT method. The goal is to find the best operating conditions such as the optimal crystal rotation that allows reducing the unwanted convective flow oscillations.

2 Numerical simulation procedure conditions

We validated our numerical simulation procedure by comparing our results with those obtained experimentally by Rahal, Cerisier and Azuma (2008).

The experimental set-up of Rahal, Cerisier and Azuma (2008) consisted of a simulated crucible made of Pyrex glass, of 10 cm inner diameter and 10 cm height, and a simulated crystal of 3 cm diameter made of brass (λ =109 W/m K at 25°C). See Figure 1). The crucible was filled with 2 cSt silicone oil (λ =0.15 W/m K at 25°C, Prandtl number, Pr = 28 at T = 25°C) as a working liquid.

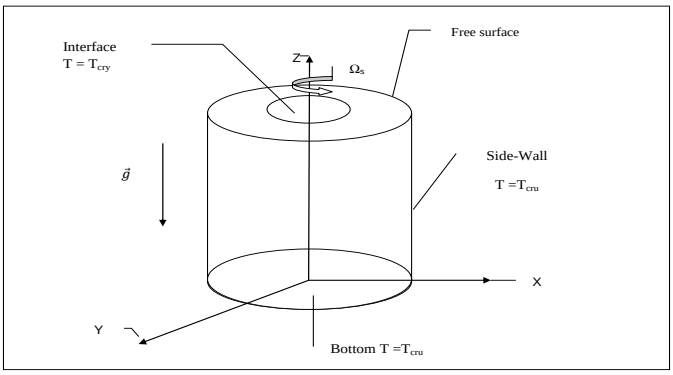

Figure 1: A Simulated Czochralski growth system

The physical properties of the 2 cSt silicone oil are given in Table 1.

Table 1: Physical properties of the 2 cSt silicone oil.

Property	Value
α	$7.1\text{x}10^{-8}\ m^2s^{-1}$
β	$0.24\text{x}10^{-3}\ K^{-1}$
λ	$0.15\ Wm^{-1}K^{-1}$
ν	$2cSt\ (2.10^{-6}\ m^2s^{-1})$
ρ	$873\ Kg\ m^{-3}$
σ	$18.7\ Nm^{-1}$
$\partial\sigma/\partial T$	$-6.28\text{x}10^{-5}\ Nm^{-1}\ K^{-1}$

The dimensions of the simulated configuration are similar to those used in the commercial Czochralski system see Kanda, Hourai, Miki, et al. (1996). The ratio of the crucible's diameter to that of the crystal is close to 3 in both cases. The Prandlt number (Pr) is close to that of the oxide melts characterized by Prandtl numbers within the 5<Pr <20 range. For that situation, the flow behavior is expected to reflect the real system.

The fluid flow and heat transport are governed by the continuity, Navier-Stokes and energy equations expressing the conservation of mass, momentum and energy. In cylindrical coordinates *(r, θ, z)*, speed will be denoted $\vec{U} = (u, v, w)$ the pressure (*P*) and temperature (T). In the Cz configuration, the free surface of the crucible and the liquid/solid interface are assumed to be flat. For an incompressible Newtonian fluid, the Navier-Stokes and energy equations under Boussinesq approximations see Bing, Xu. (2005), can be written as follows.

$$\vec{\nabla}.\vec{U} = 0$$
$$\frac{\partial \vec{U}}{\partial t} + \left(\vec{U}.\vec{\nabla}\right)\vec{U} = -\frac{1}{\rho_0}\vec{\nabla}P_m - \beta\left(T - T_0\right)\vec{g} + \nu\Delta\vec{U} \quad (1)$$
$$\frac{\partial T}{\partial t} + \left(\vec{U}.\vec{\nabla}\right)T = \alpha\,\Delta T$$

The initial conditions are the following:

$t = 0$; $u = v = w = 0$; flow is purely conductive (2)

$$\alpha\left(\frac{1}{r}\frac{\partial}{\partial r}\left(r\frac{\partial T}{\partial r}\right)+\frac{1}{r^2}\frac{\partial}{\partial \theta}\left(\frac{\partial T}{\partial \theta}\right)+\frac{\partial}{\partial z}\left(\frac{\partial T}{\partial z}\right)\right)=0$$

$$\alpha = \frac{\lambda}{\rho C_p}$$

The boundary conditions are:

Along the bottom wall ($z = 0$; $0 \le \theta \le 2\pi$ and $0 \le r \le R_{cru}$)

$$u = v = w = 0; T = T_{cru} \quad (3)$$

Along the side wall ($r = R_{cru}$; $0 \le \theta \le 2\pi$ and $0 \le z \le H$)

$$u = v = w = 0; T = T_{cru} \quad (4)$$

Along the interface ($z = H$; $0 \le \theta \le 2\pi$ and $0 \le r \le R_{cry}$)

$$u = v = 0 \ ; \ w = R_{cry}\Omega_{cry} \ ; \ T = T_{cry} \quad (5)$$

Along the free surface ($z = H$; $0 \le \theta \le 2\pi$ and $R_{cry} \le r \le R_{cru}$)

$$\frac{\partial u}{\partial z} = -\frac{1}{\mu}\frac{\partial \sigma}{\partial T}\frac{\partial T}{\partial r}; \frac{\partial v}{\partial z} = -\frac{1}{\mu r}\frac{\partial \sigma}{\partial T}\frac{\partial T}{\partial \theta}; w = 0; \ \lambda\frac{\partial T}{\partial z} = h(T - T_a) \quad (6)$$

In the present work, the numerical simulations were carried out using the commercial CFD software FLUENT 6.3. The unsteady state continuity and momentum equations are discretized over the computational domain using a finite volume method. Convection and diffusion terms are discretized by the second-order upwind schema. The SIMPLE algorithm is used to resolve the pressure-velocity coupling. The solution was checked to be independent of the grid by performing a grid independency study using four different grids. See Table 2. It is observed that there is a small difference between the profiles predicted by Grid 3 and Grid 4., See Figure 2, therefore, the Grid 3 was adopted for the present work.

Table 2: Details of the four grids used for the grid independency study

Grid	Grid 1	Grid 2	Grid 3	Grid 4
Number of nodes (10^3)	32	96	149	322

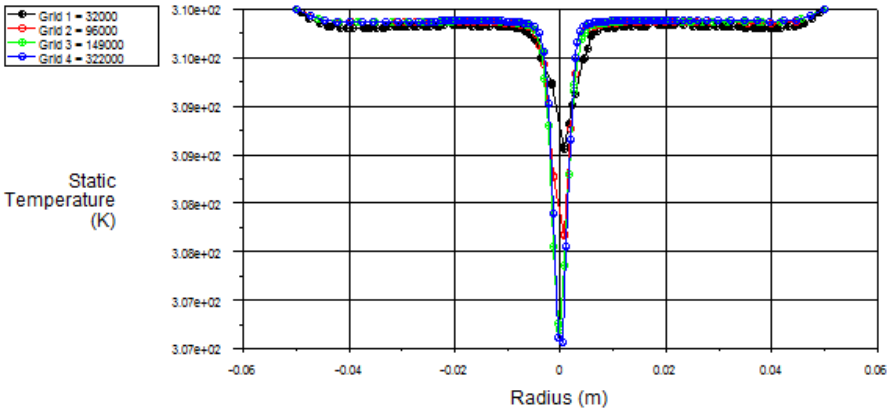
Grid 1 - 32000
Grid 2 - 96000
Grid 3 - 149000
Grid 4 - 322000
Static Temperature (K)
3.10e+02
3.10e+02
3.09e+02
3.09e+02
3.08e+02
3.08e+02
3.07e+02
3.07e+02
-0.06
-0.04
-0.02
0
0.02
0.04
0.06
Radius (m)

(a)

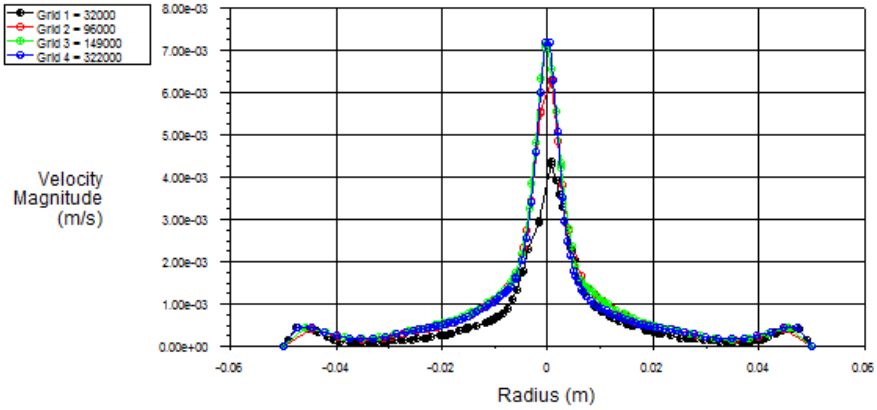
Grid 1 - 32000
Grid 2 - 96000
Grid 3 - 149000
Grid 4 - 322000
Velocity Magnitude (m/s)
8.00e-03
7.00e-03
6.00e-03
5.00e-03
4.00e-03
3.00e-03
2.00e-03
1.00e-03
0.00e+00
-0.06
-0.04
-0.02
0
0.02
0.04
0.06
Radius (m)

(b)

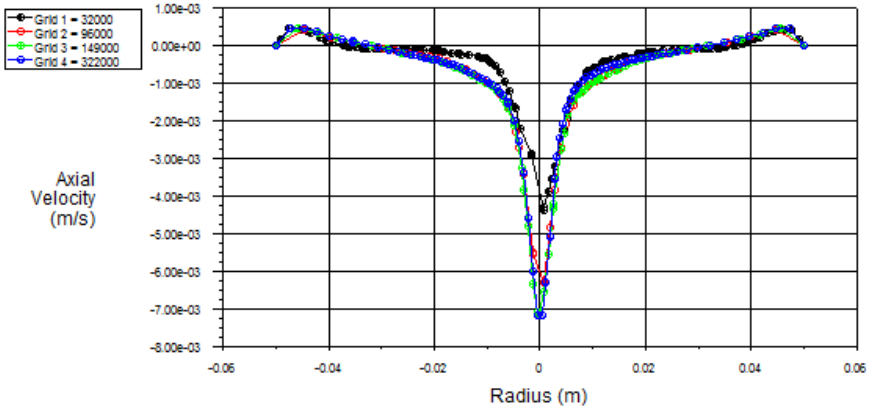
Grid 1 - 32000
Grid 2 - 96000
Grid 3 - 149000
Grid 4 - 322000
Axial Velocity (m/s)
1.00e-03
0.00e+00
-1.00e-03
-2.00e-03
-3.00e-03
-4.00e-03
-5.00e-03
-6.00e-03
-7.00e-03
-8.00e-03
-0.06
-0.04
-0.02
0
0.02
0.04
0.06
Radius (m)

(c)

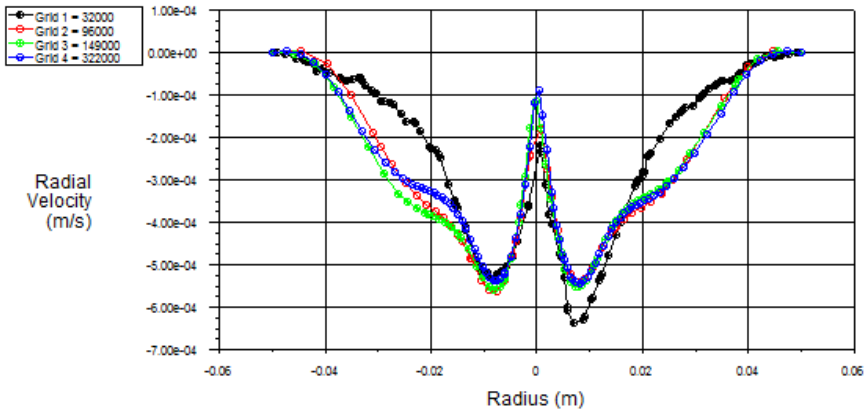

(d)

Figure 2: Results corresponding to the various grids along the radius, at z = 0.09 m (a) Static temperature; (b) Velocity magnitude, (c) axial velocity and (d) Radial velocity

The grid 3. See Figure 3. and a time step, $\Delta t = 10^{-2}$ are adopted in the numerical simulation. The geometrical and temperature parameters are taken as in Rahal, Cerisier and Azuma (2008), crystal and crucible radius are $R_{cry} = 1.5\,cm$ and $R_{cru} = 5\,cm$, liquid height is $H = 10cm$, temperature difference between the crucible wall (T_{cru}) and the crystal (T_{cry}) is ΔT=5 or 10 K.

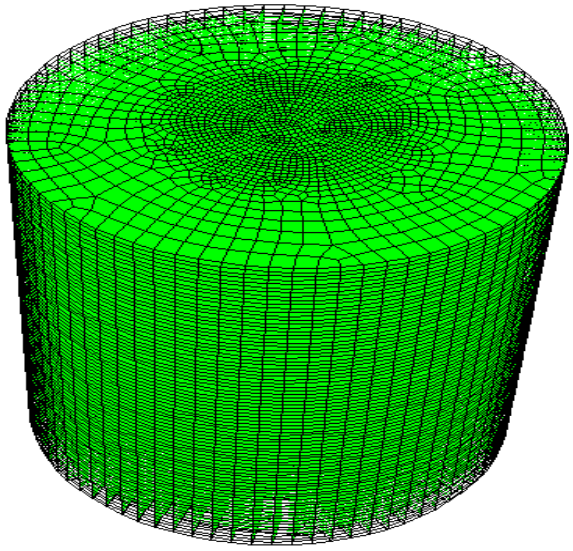

Figure 3: The grid 3 (number of nodes 149000).

The important dimensionless numbers governing the studied system are:

Prandtl number $\mathrm{Pr} = \dfrac{\nu}{\alpha}$

Marangoni number $Ma = \frac{\partial \sigma}{\partial T} \frac{(R_{cru} - R_{cry})\Delta T}{\mu \alpha}$

Rayleigh number $Ra = \frac{g\beta \Delta T \mathrm{H}^3}{\alpha \nu}$

Reynolds number $\mathrm{Re}_{cry} = \frac{\Omega_{cry} R_{cry}}{\nu}$

α Thermal diffusivity,

β Volumetric coefficient of thermal expansion

μ Dynamic viscosity,

ν Kinematic viscosity,

σ Surface tension,

$\frac{\partial \sigma}{\partial T}$ Surface tension variation as function of the Temperature,

ΔT Difference of temperature applied between the crucible and the crystal,

For the simulations conducted in this work the dimensionless numbers are as follows.

$\mathrm{Pr} = 28$

$Ma = 88.65 \times 10^3 (\Delta T = 5K)$; $17.73 \times 10^3 (\Delta T = 10K)$

$Ra = 10^7 (\Delta T = 5K)$ *and* $2.1 \times 10^7 (\Delta T = 10K)$

$\mathrm{Re}_{cry} = 0$ *to* 2900 $(\Omega_{cry}$ *from* 0 *to* 246 *rpm*$)$

3 Results and analysis

3.1 Validation of the Numerical simulation Procedure

In order to validate our numerical simulation procedure, the streamlines, at various Rayleigh and Reynolds crystal numbers, obtained using our numerical simulations, have been compared to those obtained by Rahal, Cerisier and Azuma (2008). It can be noticed that there is a good agreement. See Figure 4 and Figure 5. The flow was visualized in the vertical median plane of the crucible. In the Cz flow, the most important driving forces are the centrifugal force due to the crystal rotation; the buoyancy force due to the temperature gradient and the Marangoni convection due to the surface tension gradient. The corresponding flows are shown in Figure 4 (a) and (b), respectively. The first flow has the shape of a ring rotating around its own axis and the second one is an axisymetric flow. As a result of the combination of the flows induced by these forces, the flow behaves in a very complex manner in the crucible. See Figure 5.

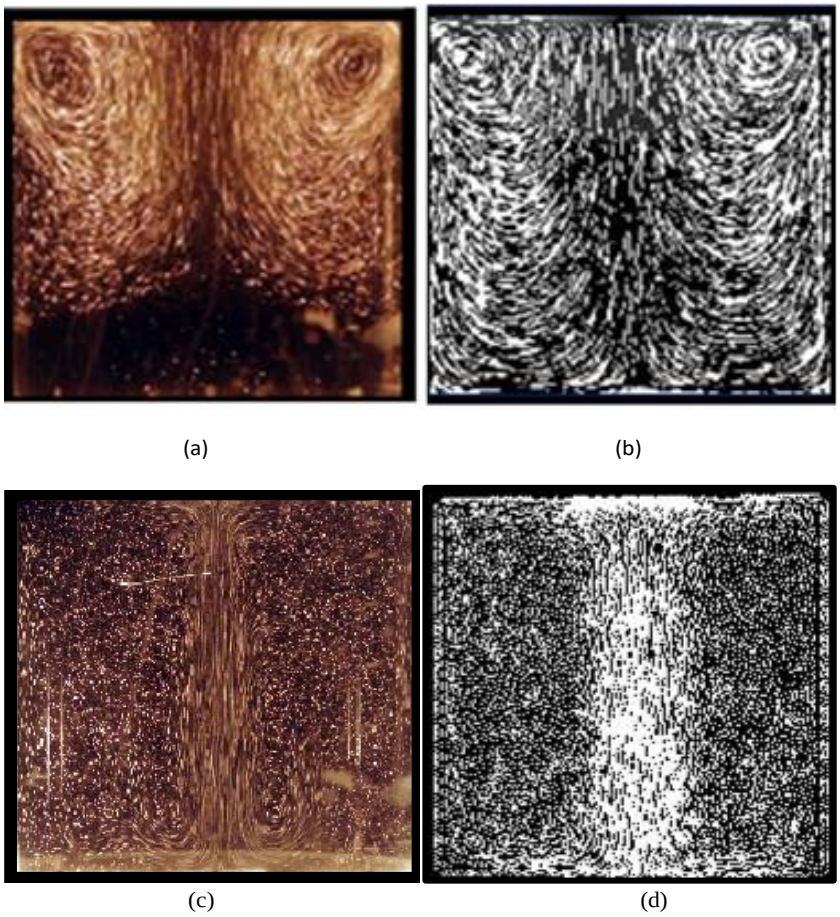

Figure 4: Observed patterns, in the crucible's vertical median plane, in 2 cSt silicone oil. (a), (c): Ra = 0, $\mathrm{Re}_{cry} = 5.9 \times 10^2$. (b), (d): Ra = 10^7, $\mathrm{Re}_{cry} = 0$. (a), (c): Experimental visualizations (Rahal, Cerisier and Azuma (2008)). (b), (d): Our results.

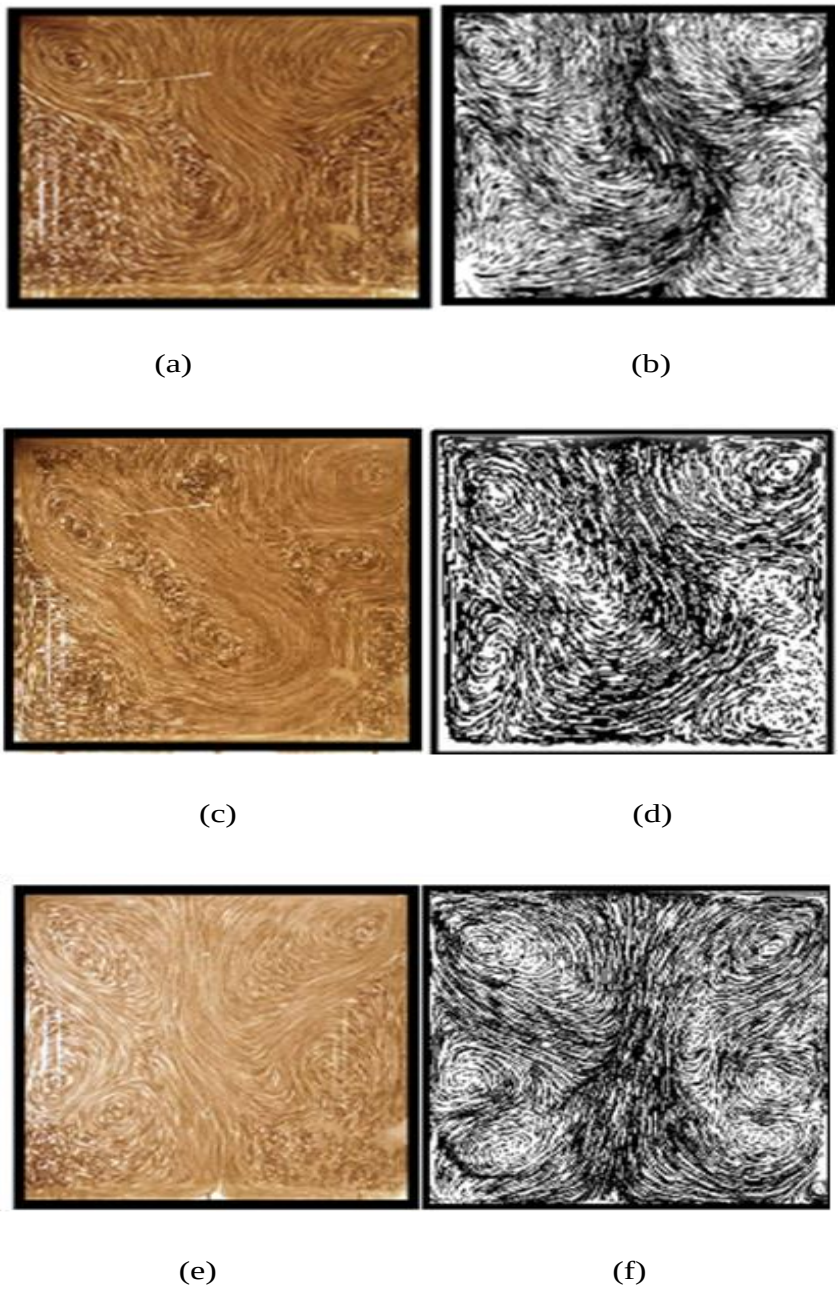

Figure 5: Observed patterns, in the crucible's vertical median plane, in 2 cSt silicone oil. (a), (b): Ra = 10^7, $\mathrm{Re}_{cry} = 1800$. (c), (d): Ra = 10^7, $\mathrm{Re}_{cry} = 2900$, (e), (f): Ra = $2.1.10^7$, $\mathrm{Re}_{cry} = 1800$. (a), (c), (e): Experimental visualizations (Rahal, Cerisier and Azuma (2008)). (b), (d), (f): Our results.

3.2 Analysis of the convective flow instabilities

The displayed Figure 6. shows the radial and tangential velocity along the line (z=0.09 m (below the solid-liquid interface) at the instant t=300 s for a series of the crystal rotation speeds (ranging from 0 to 246 rpm). For low rotational speeds<10 rpm, the radial velocity is negative and the tangential velocity is very low, which means that the flow direction is radial from the sidewalls towards the crucible axis of symmetry. Such result allowed us concluding that the free convection supported by the Marangoni convection dominates the forced convection. For such situation, the thermal and dynamic fields are axisymmetric. For large values of the crystal rotational speed (≥60 rpm), there is a change in the direction of the flow and a significant increase in the amplitude of the radial and tangential velocities. The flow becomes three-dimensional which reflects the importance of the forced convection. Zhang, Zheng and Prasad (1998) found that the asymmetrical flow in the CZ industrial system, begin for rotation speeds of about 20 to 30 rpm.

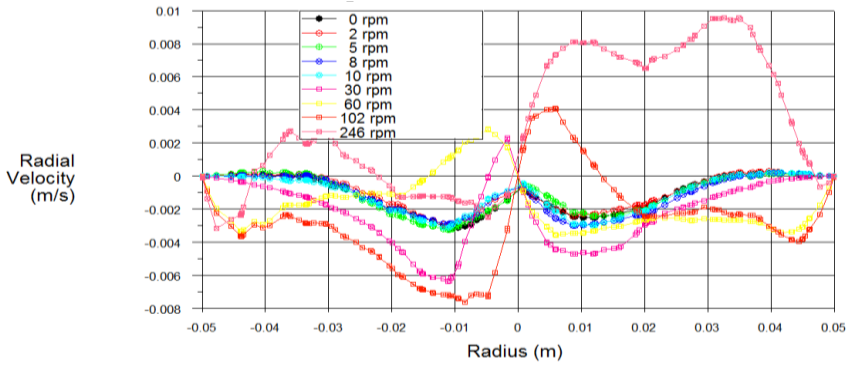

(a)

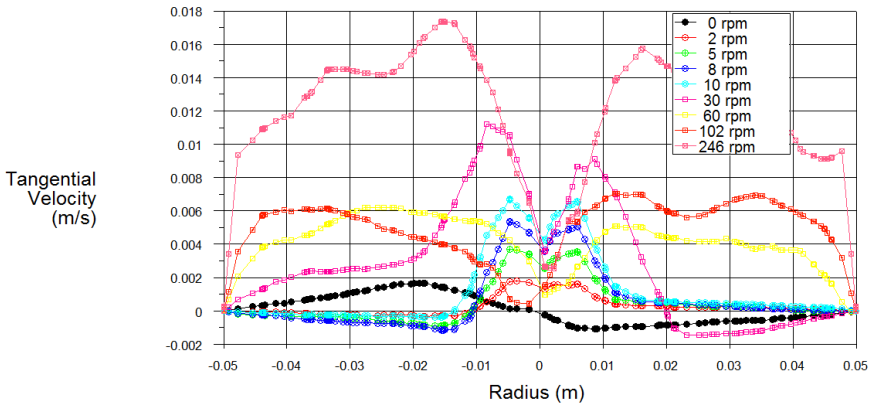

(b)

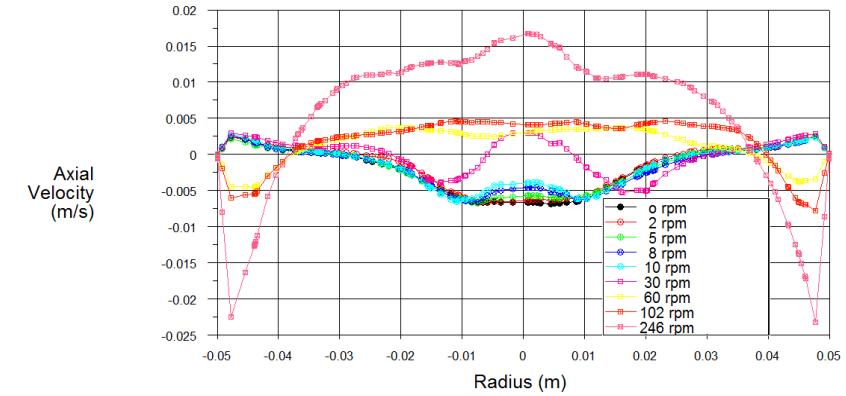

(c)

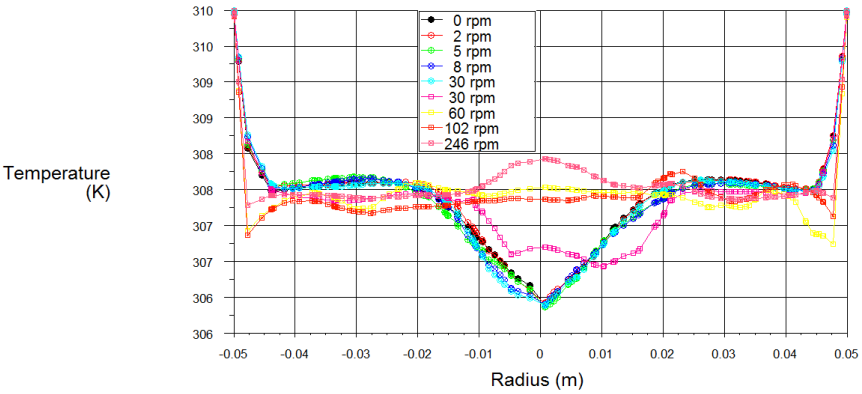

(d)

Figure 6: Radial velocities (a), tangential velocities (b), axial velocities (c), temperature; (d), along the radius at z=0.09 m for various crystal rotation rates. Ra=10^7 (ΔT=5 K).

The transient flow patterns exhibit a significant role of the Marangoni convection on the fluid flow instability at the free surface of the melt. A strong radial flow due to the presence of a surface tension effect is observed to enhance the main flow around the axis of symmetry. See Figure 7.

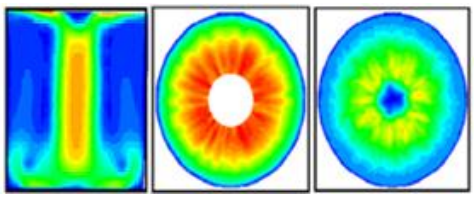

(a) (b) (c)

Figure 7: Velocity profile Ra=0 (μg=microgravity), Re=0 and Ma=88.65x10^3 (a): in the crucible's vertical median plane (b): at the free surface (c): in a cross section just below the melt free surface (z=0.095 m).

An instability mechanism consisting of a cold plume. See Figure 8., detaching from the cold crystal towards the crucible bottom, has been observed. The visualizations made by Teitel, Schwabe and Gelfgat (2008), for a Prandtl number Pr=23.9 revealed also the presence of instability "cold plume" where the cold fluid is accumulated near the crystal, then descends down.

With the increase of the temperature difference or crystal rotation, other instability mechanisms, characterized by three-dimensional oscillations were observed.

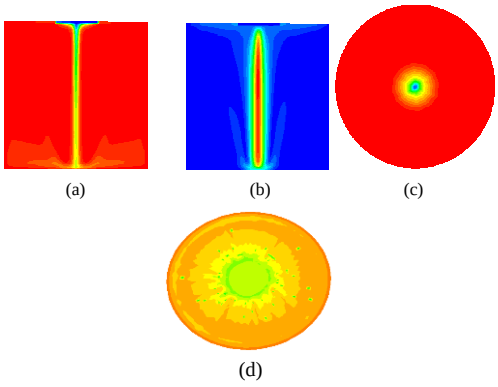

Figure 8: (a): Temperature profile at the crucible's vertical median plane. (b): Velocity profile at the crucible's vertical median plane. (c) and (d): Temperature profile at a cross section just below the melt free surface (z=0.095 m), for Ra=0, $\mathrm{Re}_{cry} = 0$ or $\mathrm{Re}_{cry} = 335$.

In order to locate the position which has large fluctuations, three positions were taken in the plane z=0.098 m (2 mm below the solid-liquid interface.) P1 (0,0,0.098), P3 (0.015,0,0.098), P4 (-0.015,0,0.098) and a position P2 (0,0,0.09) on the plane z = 0.09 m) (1 cm below the interface). For P1 and P2, the amplitudes of fluctuations are equal and higher than those found for P3 and P4 which are also of the same order. See Figure 9. P1 is then adopted for our analysis.

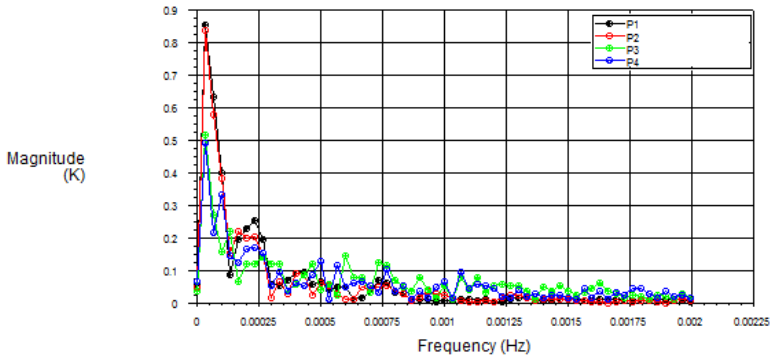

Figure 9: Power spectra of temperature fluctuations at various positions under the liquid-crystal interface.

The displayed Figure 10. shows time variation of the temperature at various crystal rotation speeds for the position P1 (z = 0.098 m) (2 mm below the cystal-liquid interface) for a series of the crystal rotation speeds (ranging from 0 to 246 rpm). For low rotational speeds (less than 10 rpm), the reached asymptotic value is the same for all speeds. For values of $10<\Omega_{cry}<30$ rpm, a gradual increase of the asymptotic value is observed until reaching a value that remains constant for speeds$\geq$60 rpm.

The FFT corresponding to the curves of Figure 10. are displayed in Figure 11. It can be noticed that for all rotational speed the spectra are continuous and higher magnitudes are observed for the lower values of the frequency. Figure 11. shows the FFT spectra of temperature fluctuations at P1 (2 mm under the interface) for various crystal rotation speeds. The oscillations depend on the considered crystal speed and they are more important for the lower speeds than for the higher ones.

As mentioned above, thermal fluctuations are detrimental to the quality of the crystal in the Czochralski system, the aim of this work is to understand their behavior in order to find the best means to control them. We have found that the use of a crystal rotational speed large than 10 rpm allows reducing the magnitude of the temperature fluctuations.

Such result is qualitatively similar to the result found by Hintz, Schwabe (2001); Chen, LI (2007).

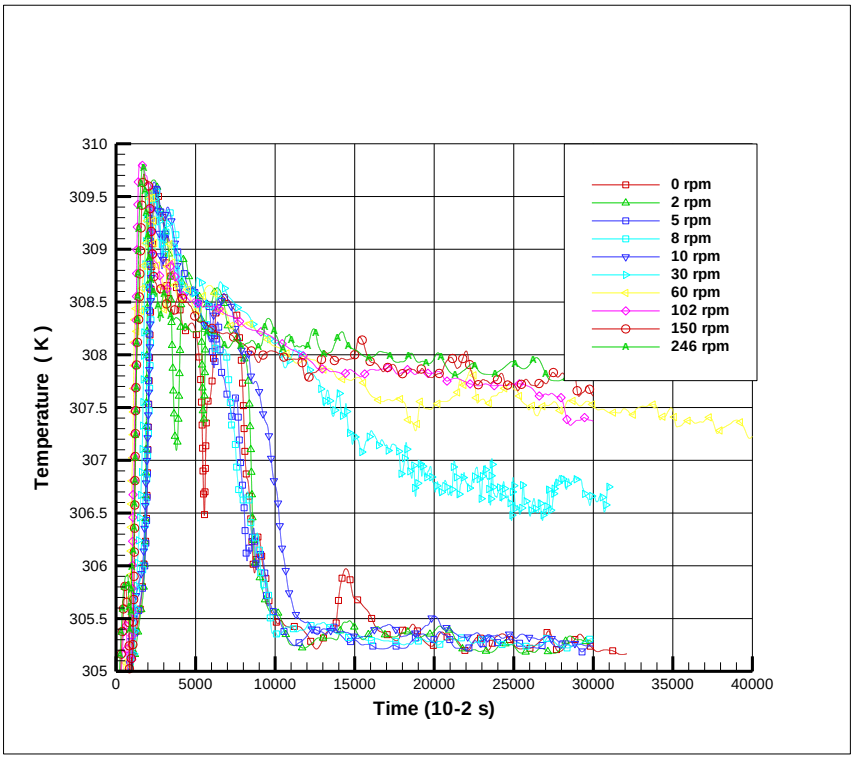

Figure 10: Time variation of the temperature at various crystal rotation speeds for the position P1.

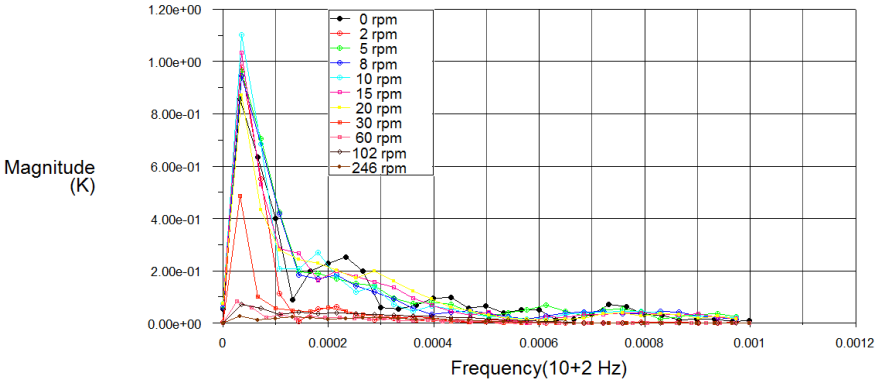

Figure 11: Fast Fourier transforms of the temperature fluctuations at P1 (2 mm below the interface) for various crystal rotation rates.

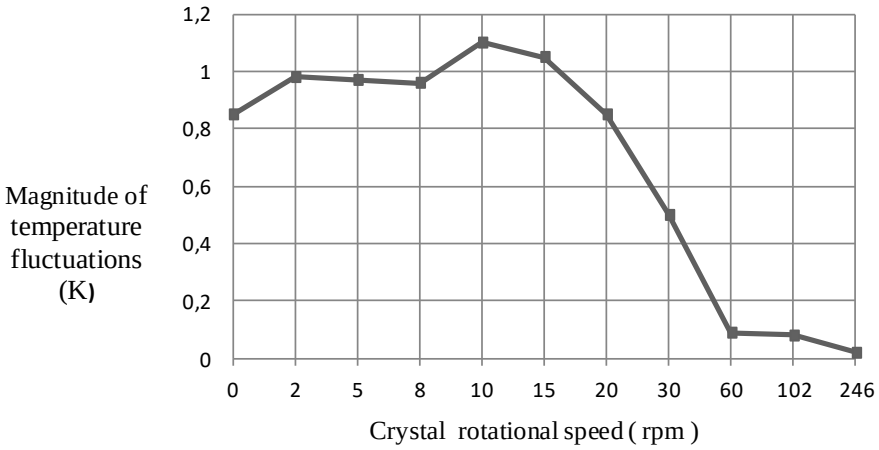

Figure 12: Magnitude of the temperature fluctuations as a function of the crystal rotational speed.

The displayed Figure 12 shows the variation of the temperature fluctuation magnitude as a function of the crystal rotational speed. At first (from speed ranging from 0 to 10 rpm), the fluctuation magnitude increases slowly until reaching its maximum value for the 10 rpm speed. Then, it decreases rapidly when the speed is varied from 10 to 60 rpm. For crystal speed larger than 60 rpm, the oscillation magnitude tends to zero.

4 Conclusions

The first part of this work is devoted to the study of the flow induced by the rotation of crystal with the presence of Marangoni convection at the free surface. In the second part, we studied the effect of the crystal rotation on the temperature fluctuations in the simulated Czochralski system. This work completed an experimental work, in which

interesting patterns were observed, and has not been previously simulated numerically.

From experiments, it has been shown that a higher crystal rotation reduces the temperature fluctuations under the crystal for fewer crystal speeds (0, 60, 102, 150 or 246 rpm) compared to the numerical study conducted in this work. The most experimental works, examined only the effect of the slow crystal rotation on three-dimensional oscillatory instability in a Czochralski melt flow. The measurements confirmed, partially the destabilization of the Czochralski convective flow by a slow rotation.

The flow transition from axisymmetric to non-axisymmetric flow in the Czochralski melt is due to the interaction between the horizontal temperature gradient and the vertical one. In the present study, the horizontal temperature gradient is more dominant than the vertical one, such fact has also been observed some authors.

Finally, and contrary to what was mentioned at the literature, about the disagreement between experimental and numerical results in the Czochralski modeling, the present numerical study is in a good agreement with the experimental work.

References

Gelfgat, A. Yu. (2007): Three-Dimensional Stability Calculations for Hydrodynamic Model of Czochralski Growth. *Journal of Crystal Growth*, vol. 303, pp. 226-230.

Haslavsky, V.; Miroshnichenko E.; Kit, E.; Gelfgat, A. Y. (2011): On experimental and numerical prediction of instabilities in Czochralski melt flow configuration. *Journal of Crystal Growth*, vol. 318, pp. 156-161.

Haslavsky, V.; Kit E.; Gelfgat, A. Y. (2013): Experimental Modeling of Czochralski Melt Flow with a Slow Crystal Dummy Rotation. *Acta Physica Polonica*, vol. 124, pp. 193-197.

Haslavsky, V.; Miroshnichenko, E.; Kit E.; Gelfgat, A. Yu. (2013): Comparison and a Possible Source of Disagreement between Experimental and Numerical Results in a Czochralski Model. *Fluid Dynamics & Materials Processing*, vol. 9, no. 3, pp. 209-234.

Hintz, P.; Schwabe D. (2001): Convection in a Czochralski crucible-Part 2: rotating crystal. *Journal of Crystal Growth*, vol. 222, pp. 356-364.

Hintz, P.; Schwabe, D.; Wilke, H. (2001): Convection in a Czochralski crucible-Part 1: non-rotating crystal. *Journal of Crystal Growth*, vol. 222, pp. 343-355.

Kakimoto, K.; Watanabe, H.; Eguchi, M.; Hibiya, T. (1994): Flow instability of the melt during Czochralski Si crystal growth: dependence on growth conditions; a numerical simulation study. *Journal of Crystal Growth*, vol. 139, pp. 197-205.

Kanda, T.; Hourai, M.; Miki, S.; Shigematsu, T.; Tomokage, H.; Miyano, T.; Morita, H.; Shintani, A. (1996): Influence of Melt-temperature Fluctuations on Striation Formation in Large-Scale Czochralski Si Growth Systems. *Journal of Crystal Growth*, vol. 166, pp. 663-668.

Li, Y. R.; Peng, L.; Shi, W. Y.; Imaishi, N. (2006): Convective Instability in Annular Pools. *Fluid Dynamics & Materials Processing*, vol. 2, no. 3, pp. 153-165.

Rahal, S.; Cerisier, P.; Azuma, H. (2008): Application of the proper orthogonal

decomposition to turbulent convective flows in a simulated Czochralski system. *International Journal of Heat & Mass Transfer*, vol. 51, pp. 4216-4227.

Chen, S. X.; Li, M. W. (2007): Flow Instability of Molten GaAs in the Czochralski Configuration. *Journal of Materials Science & Technology*, vol. 23, no. 3, pp. 395-401.

Teitel, M.; Schwabe, D.; Gelfgat A. Y. (2008): Experimental and computational study of flow instabilities in a model of Czochralski growth. *Journal of Crystal Growth*, vol. 310, pp. 1343-1348.

Xu, B. (2005): Numerical and experiment studies on convective phenomena in materials processing systems, doctoral thesis, *Mechanical Engineering*, Washington State University.

Zhang, H.; Zheng, L.; Prasad, V.; Larson, D. J. (1998): Diameter-Controlled Czochralski Growth of Silicon Crystals. *Journal of Heat Transfer*, vol. 120, pp. 874-882.

Zhong, Z.; Jingqiu, C.; Hiroshi, M. (2003): Three-dimensional oscillatory convection of LiCaAlF 6 melts in Czochralski crystal growth. *Journal of Crystal Growth*, vol. 252, no. 4, pp. 538-549.